Molecular Crystals and Liquid Crystals

Publication details, including instructions for authors and subscription information:
http://www.tandfonline.com/loi/gmcl20

Thickness Dependent Dewetting in Photosensitive Azo-Polyacrylate Langmuir Blodgett Films

L. Cristofolini [a], M. P. Fontana [a], T. Berzina [a] & P. Camorani [a]

[a] Dipartimento di Fisica and INFM, Università di Parma, Parco Area delle Scienze 7/A, Parma, 43100, Italy

Version of record first published: 18 Oct 2010

To cite this article: L. Cristofolini, M. P. Fontana, T. Berzina & P. Camorani (2003): Thickness Dependent Dewetting in Photosensitive Azo-Polyacrylate Langmuir Blodgett Films, Molecular Crystals and Liquid Crystals, 398:1, 11-22

To link to this article: http://dx.doi.org/10.1080/15421400390220836

Mol. Cryst. Liq. Cryst., Vol. 398, pp. 11–22, 2003

ISSN: 1542-1406 print/1563-5287 online
DOI: 10.1080/15421400390220836

Taylor & Francis
Taylor & Francis Group

THICKNESS DEPENDENT DEWETTING IN PHOTOSENSITIVE AZO-POLYACRYLATE LANGMUIR BLODGETT FILMS

L. Cristofolini, M. P. Fontana, T. Berzina, and P. Camorani
Dipartimento di Fisica and INFM, Università di Parma, Parco Area delle Scienze 7/A, 43100 Parma, Italy

In this paper we summarize our recent results on the self organized motion of a photosensitive polymeric liquid crystal. We studied the quality of pristine Langmuir-Blodgett molecular layers and their photoinduced dewetting. In particular, we have found that the dewetting proceeds in very different ways depending on the initial film thickness: above a certain threshold a long range molecular flow is obtained, with mass transport over macroscopic distances. The resulting morphology comprises of a wide distribution of polymeric droplets, very polydispersed in size. On the contrary, below the threshold, the self-organized dewetting motion is quasi-local, resulting in a dense and uniform distribution of droplets of similar size. Finally, we discuss the quality of the molecular layers as a function of substrate pre-treatment, and of layer composition when a fraction of monomers is introduced. We discuss these results- relevant for the confinement of glass formers in monodispersed nanoparticles- also in the framework of thickness dependent melting phenomena, trying to elucidate the eventual role of the polymer mesogenicity in determining the observed phenomenology.

Keywords: atomic force microscopy; dewetting; polymeric liquid crystals; photoinduced effects

1. INTRODUCTION

The retraction of a fluid, such as a simple liquid or a polymer above its glass transition temperature, from a non-wettable surface is a commonly observed phenomenon. Examples are the retraction of a water film from a window glass, of some inks from plastic surfaces, and so on.

This macroscopic process, also known as dewetting, is the result of local molecular interfacial interactions involving both static properties, as surface tension, and kinetic ones, like friction and slippage [1].

In polymer physics, the determination of the dewetting parameters, as the dewetted distance, the shape of the rim etc., may yield independent and accurate information on contact angle and surface tension of the fluid

[2]. Moreover, dewetting phenomena are relevant for fundamental studies related to the glass transition, as the onset of dewetting marks a regime of high molecular mobility, which in polymeric layers is related to the transition between the glassy and the undercooled liquid phases [3,4]. Finally, control of dewetting conditions, and inhibition of dewetting, is a fundamental issue for many applications.

As an example we may cite recent studies aiming at the use of photosensitive polymeric glass formers [5–8] to develop high-density all-optical read-write memories based on poly-azo-acrylates [9,10]. In a particular case we had developed a technique, based on electron beam irradiation of the first molecular layers of the film, which success fully inhibits the dewetting of the film from silicon substrate, albeit at the expense of loss of photosensitivity, at least for the first irradiated layers [11].

Dewetting is particularly relevant for molecular films deposited on a solid substrate in a metastable state, such as the Langmuir-Blodgett and Langmuir-Schaefer techniques [12,13], as they often tend to rearrange their morphology, either by recrystallization or by dewetting, in such a way as to minimize the energetically unfavourable interfaces between film and substrate and between film an air. Incidentally we note that this is not the case for films deposited by the self-assembly technique, as in this case the molecules are chemically bound to the substrate, either by the formation of hydrogen bonds, or by covalent bonds, and therefore are in a stable state. In the case of LB films thickness dependence of the dewetting is important, and is relevant to the processes governing the glass transition in these confined geometries. We have found substantial differences in the dewetting phenomenology depending on whether the film thickness is above or below a given threshold, which essentially establishes the effective dimensionality of the system which govern the morphology and its kinetics.

2. EXPERIMENTAL

The liquid crystalline polymer used was Poly[[4-pentyloxy-3′-methyl-4′(6-acryloxyexyloxy)]azobenzene] (PA4). Its synthesis and main characteristics are described elsewhere. Here we recall only that it has a calorimetric glass transition temperature T_g of 21°C, a melting temperature of 78°C, a nematic phase ending at the clearing point temperature of 96°C [5]. Upon cooling, the nematic fluid of the azobenzene side chains undercools all the way down to T_g. In our case the samples had a molecular weight $M_w = 19000$ (weight averaged) and $M_n = 12000$ (number averaged).

In this type of experiments, great care must be given to the details of preparation and deposition of LB multilayers. In particular, the samples must be as homogeneous and defect-free as possible. We found that the best results were obtained using the Langmuir-Schaefer (LS, horizontal lifting) deposition technique. The deposited films were routinely checked with an optical polarizing microscope (Zeiss Axiotech) used also in Differential Interference Contrast mode. Film thickness was independently measured by high precision null-ellipsometry (Multiskop). Mesoscopic and nanoscopic surface morphology was monitored with scanning force microscopy in non-contact mode (Park CP Autoprobe Research) using NT-MDT Si tips operating typically at 280 kHz. The experiments were performed in dark and at room temperature; particular attention was paid to the latter point: the light source for the optical observation of sample and AFM tip was used at the minimum, and it was red-filtered in order to eliminate all the green-blue components that are known to affect the azobenzene moiety. The effect of UV illumination was monitored exposing the samples kept at room temperature to the light from a high pressure Hg lamp, whose maximum emissivity is peaked at $\lambda \sim 350$ nm.

For the deposition of macroscopically and microscopically homogeneous multilayers, it is necessary to find optimal conditions for both Langmuir monolayer formation and its transfer on the substrate. We recorded the compression isotherms both in dark and under UV illumination, again provided with a Hg lamp, and deposited the films using a KSV5000 Langmuir trough of 10 cm width. In particular we prepared the sample as follows: 100 µl of chloroform solution 0.33 mg/ml of PA4 was spread on high purity water (MilliQ, $\rho > 18\,\mathrm{M\Omega cm}$), the Langmuir layer was then slowly compressed in dark at a rate of 10 mm/min up to a typical deposition pressure $\Phi = 15$ mN/m. The multilayers were deposited either on clean Si (100) surfaces, covered by natural oxide (typical thickness 20–25 Å, as determined by null-ellipsometry), or on silanized hydrophobic silicon. The wafers were first washed with soap and then cleaned in hot H_2SO_4. Silanization was performed by immersion of substrates in dimethyldichlorosilane/hexane and subsequent rinsing in hexane/acetone/hexane and final careful washing with soap and pure water. The hydrophobized substrates had a somewhat thicker oxide layer (25–30 Å by null-ellipsometry) coated by the non-polar -CH_3 group. Here we note that deposited films of best quality were obtained thanks to the rapidity of the LS deposition, which was increased in our case by the use of a horizontal grid which partitioned the polymeric monolayer into separate areas, wherein the substrate was brought in contact with the monolayer, without disturbing the surface in adjacent sections [14–15].

As stated, we deposited several types of molecular architectures. The ones we have used for this study are:

- molecular multilayers of polymer deposited at high surface pressure ($\Phi = 15$ mN/m) by the Langmuir-Schaefer technique on hydrophobic silicon substrate obtained by silanization;
- same as above deposited on hydrophilic substrate, obtained by oxidation of silicon by sulphuric acid;
- molecular monolayers deposited onto hydrophobic silicon substrate at different surface pressure, ranging from $\Phi = 1$ mN/m up to 15 mN/m

We have also deposited multilayers of mixed composition, in which a fraction of monomer of PA4 was introduced as plasticizing agent. In this case, to improve spreading quality, the monomeric fraction was dissolved in a 0.33 mg/ml solution of 2 parts of hexane for 1 part of benzene, whereas the polymeric fraction was dissolved in a 0.33 mg/ml solution of 1 part of hexane for 2 parts of benzene. The two solution where mixed in controlled proportions prior to the dispersion on the Langmuir trough.

3. RESULTS

By atomic force microscopy (AFM) we have studied the morphology and the structure of multilayers deposited onto different substrates. Monolayers deposited at high pressure ($\Phi = 15$ mN/m) onto hydrophobic substrates typically have a flat topmost surface, which can be described as being made of rigid plaques that have been pressed together, as shown in Figure 1. We can understand this by thinking that in the LS deposition process the polymeric film is pressed up to a relatively high surface pressure, and then transferred onto the solid substrate. In this process the film may break into parts. The root mean square roughness of the surface is $\sigma_{RMS} = 1$–1.5 nm. If we consider that ellipsometric and X-ray reflectivity (XRR) experiments yield an estimate of 20–22 Å per monolayer [16,17], this roughness is compatible with incomplete coverage of the topmost layer.

In Figure 2, we show the morphology of a monolayer of PA4 deposited at low surface pressure ($\Phi = 1$ mN/m). Clearly, the surface coverage is more homogeneous on the larger (micron) distances, whereas it is structured on the shorter scale, comprising of particles, of widely varying size, including very small ones, less than 5 nm in height, minimum lateral size about 10 nm. This size is compatible with polymeric coils made up of just a few chains. We consider this as an indication that at low pressure the polymeric chains retain high mobility, as it would be the case for a deposition carried out at temperatures much higher than the glass transition temperature for this material. The result is that the self attraction of the chain, possibly linked to the presence of the mesogenic side chain, causes contraction of the film at the early stage of deposition process.

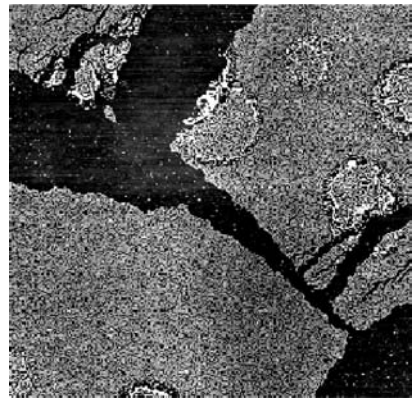

FIGURE 1 (see COLOR PLATE VI) AFM image of a single monolayer of PA4 as deposited at high surface pressure, $\Phi = 15\,\mathrm{mN/m}$. Lateral size is 10 μm, vertical contrast corresponds to 5 nm.

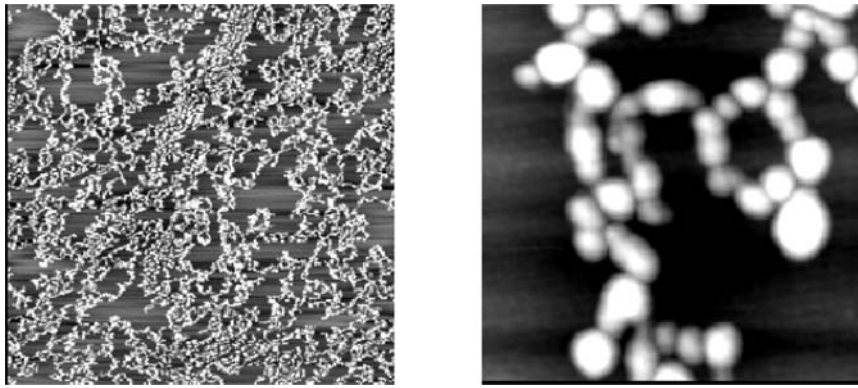

FIGURE 2 (see COLOR PLATES VII & VIII) AFM images of a single monolayer of PA4 as deposited onto hydrophobic silicon at very low surface pressure, $\pi = 1\,\mathrm{mN/m}$. **Left panel**: image size is 9 μm, **right panel**: a detail (480 nm) of the same region. In both images the vertical contrast corresponds to 10 nm.

Deposition at intermediate pressure, e.g. $\Phi = 3\,\mathrm{mN/m}$, results in poorer film morphology, with inhomogeneity on the micron scale: individual polymeric coils are merged to form dense patches of polymer, which in turn are loosely packed leaving large void spaces in between.

Coming now to the effect of UV irradiation of multilayers, its first effect, for short time exposure (less than 5 minutes in our conditions), and independently confirmed by XRR measurements [16], is the smoothing of the surface thus reducing its root mean square roughness σ_{RMS} by a factor

of 2, passing from $\sigma_{RMS} = 1$–1.5 nm to $\sigma_{RMS} = 0.6$–0.7 nm. It is remarkable that different techniques, one probing the reciprocal space, one the direct space, yield almost the same quantitative results: from the damping of Kiessig fringes in the XRR data, in the Nevot-Croce approximation, we obtained $\sigma_{RMS} = 2.0(2)$ nm before photoperturbation and $\sigma_{RMS} = 1.0(2)$ nm after photoperturbation [17]. In addition, AFM imaging provides direct microscopic description of how such smoothing effect takes place.

In Figure 3 we report for comparison the surface of a film made of 24 monolayers, before and after exposure to UV irradiation. Detailed inspection reveals how such smoothing takes place: the border of the plaques become smoother and less pronounced. Therefore the photoinduced smoothing is a consequence of higher molecular mobility, related to the presence of a large fraction of azobenzene moieties in the *cis* conformation. This was already hypothesized to explain optical data [18] and Quartz Crystal Microbalance data [8], and it correlates with our finding on the photoinduced depression of the vibrational density of states in the region of the Boson Peak as probed by inelastic neutron scattering on the same compound [19]. Additionally, as a consequence of photoperturbation, we observe the formation of particles 20–30 nm in height, which seem to lay on top of the LB multilayer.

Prolonged exposure of the multilayer to UV radiation results in retraction of the film from the surface. The same process is encountered upon heating of the same LB multilayers. Its occurrence at RT under UV illumination is again related to the above mentioned fluidification effects

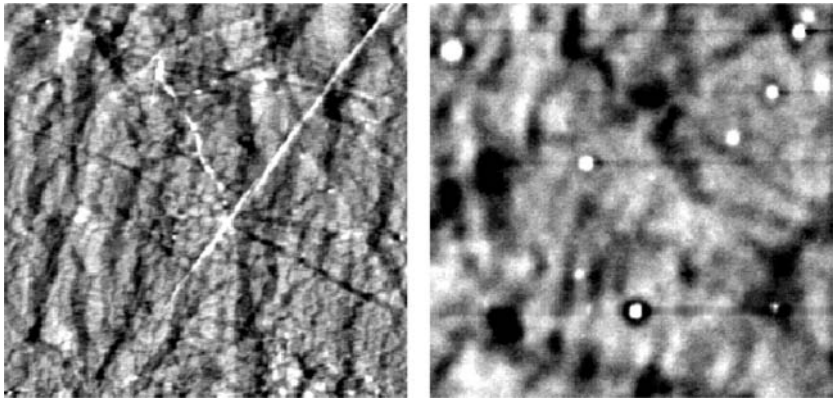

FIGURE 3 (see COLOR PLATES IX & X) AFM images of the photoinduced smoothing effect on a film comprising of 24 monolayers of PA4 here shown before (**left panel**) and after (**right panel**) exposure to UV irradiation. In both images the scanned area is 27 μm, and the vertical contrast corresponds to 5 nm.

related to the presence of a large fraction of azobenzene in the ***cis*** conformation. By taking careful images in the early stages of the dewetting process, we could assess that this process originates from defects of the film (see Fig. 4), which act as centre of nucleation for the subsequent dewetting process. In the early stages of the process the film is retracted to form a mountain, for the mass-conservation a round depressed region is left all around, whose rims subsequently retract thus leaving a craterwith one mountain in the middle, as it is beautifully illustrated in the right panel of the same Figure 4.

But it is in the final stages of the dewetting process that the more remarkable effects appear: for film of small thickness (up to 4 monolayers in our case) the final morphology consists of a uniform distribution of droplets of homogeneous height (5–10 nm) and lateral size, with an average diameter approximately 150–200 nm, spaced each other by a distance roughly equal to their size, as it is shown in Figure 5. It is remarkable that such narrow distribution of material droplets is retained even after prolonged exposure to UV irradiation: we observed its stability for exposure times up to at least 45 minutes. One could imagine that at some point anchoring on the substrate occurs, and that the small droplets cannot diffuse and merge into larger volumes.

From the average spacing between the droplets we can estimate that polymeric chain migration extends at most to 100–200 nm, roughly half of the inter-droplet separation, which however is a large distance if compared with the typical chain length, as the extended length of a typical a chain comprising of 50 monomeric units would be about 20 nm. This would imply

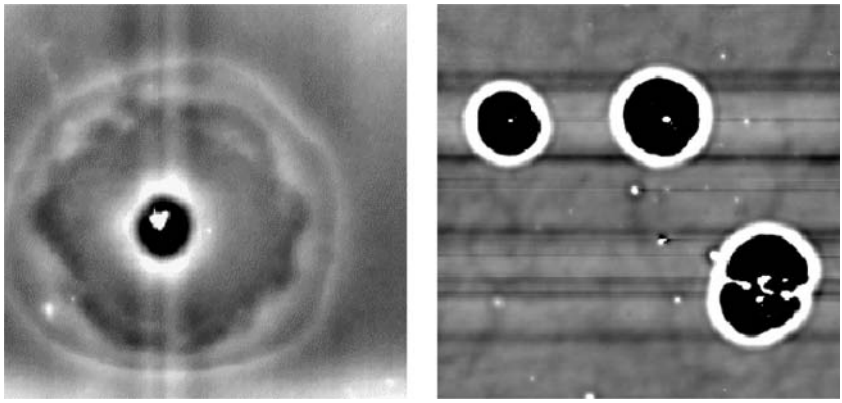

FIGURE 4 (see COLOR PLATES XI & XII) **Left**: image of the first stage of dewetting of a multilayer of PA4. The measured area is $8 \times 8\,\mu m^2$, vertical contrast scale corresponds to 35 nm. **Right**: a later stage of the dewetting process, lateral size is 50 μm, vertical contrast is 50 nm.

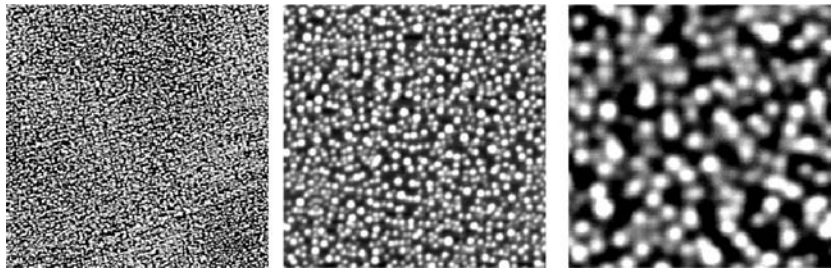

FIGURE 5 (see COLOR PLATES XIII, XIV & XV) Final stage of dewetting of a thin film comprising of 4 monolayers of PA4 under the effect of photoperturbation. **Left**: lateral size is 32 μm, vertical contrast 5 nm, **middle**: lateral size is 10 μm, **right**: detail of an area of 4 μm.

that the basic process involved is diffusion limited aggregation, which should yield a fractal-like morphology [20]. The homogeneity of the distribution indicates instead that in the confined geometry determined by the small thickness the system is essentially two-dimensional (see the forthcoming discussion).

Thicker films exhibit a quite different behaviour, as the motion of the film persists for longer exposure time resulting in material reorganization over large distances, until very large droplets are formed, some of them exceeding 10 μm in size. An optical microscope photograph is shown in Figure 6, where one can also evaluate the huge size polydispersity ranging from very small droplets of lateral size 150–200 nm (not visible in the pictures, but measured by AFM and found in all the regions not occupied

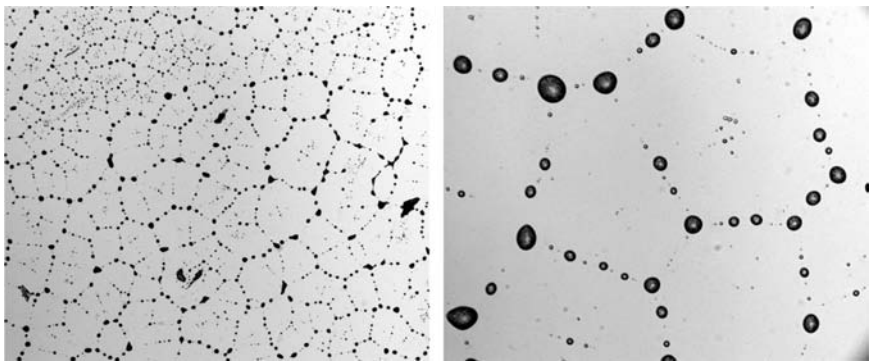

FIGURE 6 Optical microscope images of the final states of the dewetting of a thick film comprising of 24 monolayers of PA4. **Left**: magnification 10X, field of view is 1024 × 853 μm. **Right**: detail at magnification 50X, field of view is 205 171 μm.

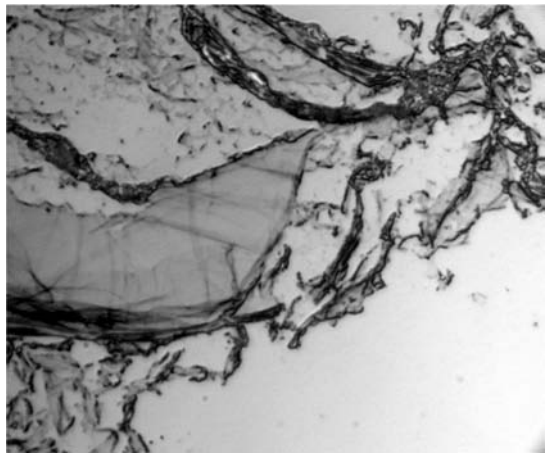

FIGURE 7 Optical microscope image (magnification 100X, field of view $105 \times 87 \mu m$) of PA4 onto hydrophilic substrate. Clearly the deposition process is poor, as can be evaluated by the non uniform coverage of the surface. White areas are uncovered substrate, black ones are collapsed film, while only the grey ones correspond to film covering the substrate.

by the larger droplets) up to almost macroscopic droplets larger that 10 μm, clearly visible in the pictures.

Coexistence of nano-dewetting with conventional mesoscopic dewetting was already observed e.g. in polystyrene films by a combination of X-ray scattering and AFM, and interpreted as the result of the dewetting of a remaining ultra-thin polymeric layer, as predicted in the framework of spinodal decomposition [21].

Here we wish to point out that the larger thickness has a non-trivial, profound effect on the observed morphology. Essentially, the system is to all effects three dimensional; thus the diffusion limited molecular processes can sustain a multi stage dewetting process. In the first stage holes are formed, possibly around some defects, or around crystallization nuclei. Next the holes grow to form the structures shown in Figure 4, left panel, and finally the rims coalesce to leave filaments only, which finally convert into ordered droplets, as can be seen in Figure 6.

The same diffusion process in not sustainable for smaller film thickness, which then is more like a frozen-liquid structure.

Incorporation of a fraction of monomeric component into the polymeric film improves the LB film quality, probably as a result of plasticizing effect that reduces film rigidity, reducing the occurrence of the cracks on the surface. However the main features of the subsequent dewetting process seem to be not affected by the presence of a fraction of monomers in the

film. Only once it occurred to us to observe the remarkable retraction of a single molecular layer from the top surface of a relatively thick film.This happened in the dark, and again is indication of the plasticizing effect of the monomeric fraction, which acts the same role as the increased temperature or the isomerised *cis* fraction of azobenzene moieties induced by the photoperturbation.

Finally we have also tested the effect of a hydrophilic substrate. We have found that the deposited film is intrinsically metastable and dewetting occurs spontaneously already at RT and without any photoperturbation. In Figure 7 we report an optical microscope photograph of such a film: only part of the surface is properly covered by the molecular film (grey areas), while large areas (white in the image) are not covered by the molecular film, which in turn has formed blobs of material (black in the image).

4. CONCLUSIONS

In discussing these results we must recall that we are dealing with a fragile glass former, and that the measurements are taken in the immediate vicinity of the glass transition temperature (just a few degrees above). Recently De Gennes and coworkers [22] have proposed a model of dewetting in ultrathin polymeric films near the glass transition, in which an important role is played by viscoelasticity and molecular mobility. Our results are in good qualitative agreement with the predictions of the model. Moreover, the thickness dependence we observe indicates a strong role of the system effective dimensionality. We refer in particular to the qualitative differences in the dewetting process at the two studied thicknesses. At the higher thickness the system is to all effects three dimensional and undergoes a spinodal decomposition in agreement with previous results on ultrathin polymeric films [21]. In particular the observed morphology is split into a quasicrystalline disposition of droplets, as a final stage of the dewetting process, and a low density distribution of small particles (maximum dimension about 200 nm diameter, 5 nm height). At the lower thickness the particle size is determined by the spatial confinement due to the film thickness itself. In this case spinodal decomposition can not take place, indicating an effective two-dimensionality of the particle aggregate. This explains the relatively homogeneous particle size distribution.

Another important point concerns the fact that we induced the dewetting isothermally, by optically pumping the *cis-trans* photoisomerization transition of the nematic azobenzene side chain. This eliminates all possible contributions to the morphology kinetics which are connected to temperature changes, thus allowing the study of the pure dewetting phenomena.

In conclusion, we have used atomic force microscopy to monitor the morphology of Langmuir Schaefer multilayers of a polymeric glass former, as a function of substrate nature, of film composition and of other parameters, and we have found optimal conditions for film deposition. Subsequently we have monitored photoinduced dewetting of the same molecular multilayers from the substrate, finding two different regimes: for large thickness collective motion is obtained, with mass transport over macroscopic distances. The resulting morphology comprises of a wide distribution of polymeric droplets very polydispersed in size. On the contrary, below the threshold, the self-organized dewetting motion is local, resulting in a dense and uniform distribution of droplets of similar size. This finding implies that collective lateral motion takes place only when the system vertical size is larger than a certain threshold, which we place between 4 and 10 monolayers (8 and 20 nm thickness), whereas below such threshold pseudo-localization occurs. These results are coherent with a recently proposed dewetting model [22].

Finally our results are relevant to the study of the glass transition in confined geometry, as we have optimised a recipe for the confinement of a polymeric fragile glass former in nanometric particles which are quite monodispersed in size.

REFERENCES

[1] de Gennes, P. G. (1985). *Rev. Mod. Phys.*, *57*, 827.
[2] Reiter, G. & Khanna, R. (2000). *Phys. Rev. Lett.*, *85*, 2753.
[3] Jones, R. A. L. & Richards, R. W. (1999). *Polymers at Surfaces and Interfaces*, Cambridge University Press: Cambridge.
[4] Keddie, J. L. & Jones, R. A. L. (1994). *Europhys. Lett.*, *27*, 59.
[5] Angeloni, A. S., Caretti, D., Carlini, C., Chiellini, E., Galli, G., Altomare, A., Solaro, A., & Laus, M. (1989). *Liquid Crystals*, *4*, 513.
[6] Hvilsted, S., Andruzzi, F., & Ramaujam, P. S. (1992). *Optics Letters*, *17*, 1234.
[7] Hvilsted, S., Andruzzi, F., Kulima, C., Siesler, H. W., & Ramanujam, P. S. (1995). *Macromolecules*, *28*, 2172.
[8] Cristofolini, L., Facci, P., Camorani, P., & Fontana, M. P. (1999). *J. Phys.: Cond. Matter*, *11*, A359.
[9] Patanè, S., Arena, A., Allegrini, M., Andreozzi, L., Faetti, M., & Giordano, M. *Optics Comm.*, in press
[10] Arisi, S., Camorani, P., Cristofolini, L., Fontana, M P., & Laus, M. (2001). *Mol. Cryst. Liq. Crystal.*, *372*, 241.
[11] Cristofolini, L., Arisi, S., & Fontana, M. P. (2002). *Synth. Metals*, *124*, 151.
[12] (1990). In: *Langmuir-Blodgett Films*, Roberts, G. (Ed.), Plenum Press: New York.
[13] (1991). In: *Ultrathin Organic Films*, Ulman, A. (Ed.), Academic Press: Boston.
[14] Lvov, Yu. M., Gurskaya, O. B., Berzina, T. S., & Troitsky, V. I. (1989). *Thin Solid Films*, *182*, 283.
[15] Lvov, Yu. M., Troitsky, V. I., & Feigin, L. A. (1989). *Mol. Cryst. Liq. Cryst.*, *172*, 89.
[16] Cristofolini, L., Fontana, M. P., & Konovalov, O. (2002). *Philos. Mag.*, *B82*, 523.

[17] Cristofolini, L., Fontana, M. P., Berzina, T., & Konovalov, O. (2002). *Phys. Rev.*, ***E***, in press.
[18] Camorani, P., Cristofolini, L., Galli, G., & Fontana, M. P. (2002). *Mol. Cryst. Liq. Cryst.*, *375*, 175.
[19] Cristofolini, L., Fontana, M. P., Laus, M., & Frick, B. (2001). *Phys. Rev.*, ***E64***, 061803.
[20] Nakayama, T., Yakubo, K., & Orbach, R. L. (1994). *Rev. Mod. Phys.*, ***66***, 381.
[21] Müller-Buschbaum, P. & Stamm, M. (1998). *Physica*, ***B248***, 229.
[22] Saulnier, F., Raphaël, E., & de Gennes, P. G. (2002). *Phys. Rev. Lett.*, *88*, 196101.